JOURNAL OF VIROLOGY, July 2011, p. 6136–6147 Vol. 85, No. 13
0022-538X/11/$12.00 doi:10.1128/JVI.00202-11

CXCR3-Dependent Plasma Blast Migration to the Central Nervous System during Viral Encephalomyelitis▽

Cristina P. Marques,[1] Parul Kapil,[1] David R. Hinton,[2] Claudia Hindinger,[1]† Stephen L. Nutt,[3] Richard M. Ransohoff,[1] Timothy W. Phares,[1] Stephen A. Stohlman,[1] and Cornelia C. Bergmann[1]*

Department of Neurosciences, Lerner Research Institute, The Cleveland Clinic, Cleveland, Ohio 44195[1]; Department of Pathology, Keck School of Medicine, University of Southern California, Los Angeles, California 90033[2]; and The Walter and Eliza Hall Institute of Medical Research, Parkville, Victoria 3050, Australia[3]

Received 28 January 2011/Accepted 4 April 2011

Immunoglobulin in cerebral spinal fluid and antibody secreting cells (ASC) within the central nervous system (CNS) parenchyma are common hallmarks of microbial infections and autoimmune disorders. However, the signals directing ASC migration into the inflamed CNS are poorly characterized. This study demonstrates that CXCR3 mediates CNS accumulation of ASC during neurotropic coronavirus-induced encephalomyelitis. Expansion of CXCR3-expressing ASC in draining lymph nodes prior to accumulation within the CNS was consistent with their recruitment by sustained expression of CXCR3 ligands during viral persistence. Both total and virus-specific ASC were reduced greater than 80% in the CNS of infected CXCR3$^{-/-}$ mice. Similar T cell CNS recruitment and local T cell-dependent antiviral activity further indicated that the ASC migration defect was T cell independent. Furthermore, in contrast to the reduction of ASC in the CNS, neither virus-specific ASC trafficking to bone marrow nor antiviral serum antibody was reduced relative to levels in control mice. Impaired ASC recruitment into the CNS of infected CXCR3$^{-/-}$ mice coincided with elevated levels of persisting viral RNA, sustained infectious virus, increased clinical disease, and mortality. These results demonstrate that CXCR3 ligands are indispensable for recruitment of activated ASC into the inflamed CNS and highlight their local protective role during persistent infection.

Antibody secreting cells (ASC), comprising both terminally differentiated plasma cells as well as their plasma blast precursors, are integral to both primary and secondary immune humoral responses against invading pathogens. Antigen encounter in draining lymph nodes induces mature B cells to proliferate and migrate to extrafollicular foci or to lymphoid follicles (21, 33). Extrafollicular B cells differentiate into short-lived ASC, which provide an early source of low-affinity circulating antibody (Ab). In contrast, activated B cells migrating to lymphoid follicles form germinal centers, where they undergo clonal expansion and affinity maturation and differentiate into either ASC or memory B cells. As infections are resolved, germinal center plasma blasts give rise to long-lived plasma cells residing primarily in bone marrow (21, 33, 34, 36). By providing survival niches for fully differentiated ASC, the bone marrow maintains serum Ab protective against reinfection.

ASC can also survive in nonlymphoid tissues following inflammatory insults. Neuroborreliosis, neurosyphilis, subacute sclerosing panencephalitis, and multiple sclerosis are all characterized by central nervous system (CNS) accumulation of ASC and/or elevated immunoglobulin in cerebral spinal fluid (7, 24, 25). During experimental CNS infections, particularly by RNA viruses such as Sindbis, Semliki Forest, rabies, and neurotropic coronaviruses, ASC appear to play a local protective role (6, 8, 11, 16, 17, 26, 31, 40). Despite numerous reports describing intrathecal humoral responses in microbial CNS infections, very little is known about the kinetics, origin, and differentiation of ASC in this or other specialized microenvironments.

During chronic CNS inflammation, B cell differentiation and sustained humoral responses are attributed to ectopic lymphoid follicle formation (7, 25). However, ASC emerge within days or weeks following microbial CNS infections, possibly contributing to immune control (8, 11, 26, 37, 40). The kinetics of virus-specific ASC recruitment suggest that these cells arise from immature ASC or memory B cells emigrating from draining lymphoid organs. However, chemokine-mediated recruitment of ASC into the CNS has not been assessed. CXCR4, CXCR5, and CCR7 expression on naïve B cells is retained during activation in follicles (3, 9). As B cells differentiate into ASC and emigrate from lymphoid follicles, CXCR5 and CCR7 downregulation reduces responsiveness to their respective ligands, CXCL13, CCL19, and CCL21. In contrast, CXCR4 expression is upregulated during ASC differentiation, and interaction with its ligand, CXCL12, is required for ASC homing and survival of mature plasma cells within bone marrow (21, 22). Migration of ASC toward CXCR3 ligands *in vitro* (10) further supports the trafficking capacity to tissues expressing its ligands CXCL9, CXCL10, and CXCL11. Although CXCR3 ligands are frequently associated with ASC in chronically inflamed tissues (21, 27, 38, 39), the biological relevance remains speculative.

* Corresponding author. Mailing address: Department of Neuroscience, Lerner Research Institute, The Cleveland Clinic, 9500 Euclid Avenue, NC30, Cleveland, OH 44195. Phone: (216) 444-5922. Fax: (216) 444-7927. E-mail: bergmac@ccf.org.

† Present address: Department of Neurology, University Hospital Carl Gustav Carus, Dresden University of Technology, 01307 Dresden, Germany.

▽ Published ahead of print on 20 April 2011.

The present study examined the role of CXCR3 in mediating ASC recruitment into the CNS of mice infected with a sublethal JHM strain of neurotropic coronavirus (JHMV). Following infection, acute encephalomyelitis resolves into a persistent infection associated with chronic immune-mediated demyelination (1). T cell-dependent clearance of infectious virus occurs within 2 weeks, independent of humoral immunity (1). Persistence is characterized by declining levels of viral RNA; however, the absence of antiviral Ab results in infectious virus recrudescence (17, 32). Delayed, but not permanent, prevention of viral reemergence by passive antiviral Ab transfer further implicated a vital role for CNS-localized ASC in controlling persistent infection (31). Transient responsiveness of ASC to CXCR3 ligands *in vitro* (10), together with sustained expression of CXCR3 ligands during CNS accumulation of virus-specific ASC in the CNS (27, 38), provided the basis to examine the role of CXCR3-mediated signaling in regulating ASC recruitment to the CNS. The results demonstrate that CXCR3 is critical for ASC migration into the inflamed CNS but not the bone marrow. Furthermore, the importance of intrathecal ASC in preventing CNS viral recrudescence is highlighted by the impaired ability of CXCR3$^{-/-}$ mice to control persisting virus, despite unimpaired antiviral serum Ab.

MATERIALS AND METHODS

Mice, virus infections, and virus titers. Homozygous CXCR3$^{-/-}$ mice, backcrossed to C57BL/6J mice for 11 generations (18), and heterozygous Blimp-1-GFP$^{+/-}$ transgenic C57BL/6J mice expressing green fluorescent protein (GFP) under the control of Blimp-1 regulatory elements (13) were housed and bred locally. C57BL/6 control mice were purchased from the National Cancer Institute (Frederick, MD). Mice of both sexes were injected intracerebrally between 7 to 8 weeks of age with 250 PFU of the glia-tropic monoclonal Ab (MAb)-derived variant of the mouse hepatitis virus strain JHMV, designated 2.2v-1 (1, 5). All procedures were carried out in accordance with Institutional Animal Care and Use Committee Guidelines. Infectious virus was determined by plaque assay from clarified spinal cord homogenates of individual mice, as described previously (29).

Isolation of mononuclear cells and flow cytometry. Spinal cords from groups of 4 to 6 mice perfused with phosphate-buffered saline (PBS) were homogenized in Tenbroeck homogenizers, and cells were recovered from the 30/70% interface of a Percoll (Pharmacia, Piscataway, NJ) step gradient following centrifugation at 850 × *g* for 40 min at 4°C, as described previously (29, 38). Single-cell suspensions from cervical lymph nodes (CLN), spleens, and femurs for bone marrow were prepared as described previously (37, 38). Pooled cells were analyzed for surface markers as described previously (29, 38) using a MAb specific for CD45 (clone Ly-5), CD4 (clone GK1.5), CD8 (clone 53-6.7), CD19 (clone 1D3), CD138 (clone 281-2), CXCR4 (clone 2B11), Ly-6G (clone 1A8) (all from BD Biosciences, Mountain View, CA), CXCR3, and CXCR2 (both from R&D Systems, Minneapolis, MN). Virus-specific CD8$^+$ T cells were identified using H-2D^b-S510 major histocompatibility complex (MHC) class I tetramers (29). Samples were analyzed using a FACSCalibur flow cytometer (BD Biosciences) and FlowJo software (TreeStar Inc., Ashland, OR).

ASC ELISPOT assays, serum Ab, and CNS Ab. Total and JHMV-specific immunoglobulin (Ig) G ASC were detected by enzyme-linked immunospot (ELISPOT) assay as described previously (37, 38). Briefly, 96-well plates were coated with either virus (~5 × 10^5 PFU/well) or polyclonal goat anti-mouse Ig (10 μl/ml; Cappel Laboratories, Inc., Cochranville, PA). Serial dilutions of cells plated in triplicate were incubated for 4 h at 37°C. ASC were detected by sequential incubation with biotinylated rabbit anti-mouse IgG (0.5 μg/ml; Southern Biotech, Birmingham, AL) overnight at 4°C, avidin peroxidase (2 μg/ml; Sigma, St. Louis, MO) for 1 h at room temperature, and filtered 3,3′-diaminobenzidine substrate (~3 min). Spots were counted using an ImmunoSpot ELISPOT reader (Cellular Technology Ltd., Shaker Heights, OH).

JHMV-specific IgG2a serum Ab was quantified by ELISA as described previously (29, 37) using biotinylated goat anti-mouse IgG2a as the detection Ab (0.5 μg/ml; Southern Biotech). Titers are expressed as the log of the highest dilution with an optical density (OD) value exceeding 3 standard deviations above the mean background. Neutralizing Ab was measured as described previously (37, 38). Briefly, following heat inactivation, triplicates of serial 2-fold dilutions of pooled serum from 3 to 5 mice were incubated with 50 PFU of JHMV in 96-well plates for 90 min at 37°C. DBT cells (9 × 10^4 cells/well) were added, and plates were incubated at 37°C for 48 h. Neutralization titers represent the log of the highest average serum dilution that inhibited cytopathic effect.

JHMV-specific IgM and IgG titers within the CNS were determined in clarified spinal cord supernatants from individual mice by ELISA as described for serum above. Briefly, 96-well plates were coated with 100 μl of serum-free JHMV and washed with PBS containing 0.05% Tween 20, and nonspecific binding was blocked with 10% fetal calf serum (FCS) in PBS overnight at 4°C. Samples were added at 2-fold dilutions and incubated overnight at 4°C. Bound IgM or IgG was detected using biotinylated goat anti-mouse IgM (Jackson ImmunoResearch, West Grove, PA) or goat anti-mouse IgG2a (Southern Biotech). Following a 2-h incubation at room temperature, secondary Ab was detected using streptavidin-horseradish peroxidase (HRP; BD Pharmingen), followed by 3,3′,5,5′-tetramethylbenzidine (TMB Reagent Set; BD Bioscience). Optical densities were read at 450 nm in a Bio-Rad model 680 microplate reader and analyzed using Microplate Manager, version 5.2, software (Bio-Rad Laboratories, Hercules, CA). Data are expressed as arbitrary units per tissue where 1 arbitrary unit is equivalent to 0.1 absorbance. Levels were calculated using the following formula: (absorbance at 450 nm/0.1) × dilution factor × total volume of clarified CNS supernatant (3 ml per spinal cord). Background values obtained from naïve mice were subtracted. Typical dilutions resulting in linear optical density readings started at 1:80 or 1:160 for IgG and at 1:10 or no dilution for IgM at days 21 and 28 postinfection (p.i.).

Gene expression, cytokine analysis, and immunohistochemistry. Frozen tissue was homogenized in TRIzol reagent (Invitrogen, Carlsbad, CA) using a TissueLyser and stainless steel beads (Qiagen, Valencia, CA). RNA was extracted according to the manufacturer's instructions, DNase treated, and reverse transcribed as described previously (27, 28). Gene expression was quantified using a 7500 Fast Real Time PCR system (Applied Biosystems). SYBR green Master Mix (Applied Biosystems, Foster City, CA) and previously described primers were used for transcripts encoding CXCL9 (14, 38), CXCL10 (14, 38), IL-21 (27), and JHMV nucleocapsid protein (29). Primers for CXCL1, CXCL2, and CXCL12, respectively, were the following: forward, 5′-ACAGTCCCGCTG ACCAAGAG-3′, and reverse, 5′-CACTGACAGCGCAGCTCATT-3′; forward, 5′-GCAAGTGCTCCAATCTTGCA-3′, and reverse, 5′-CTTCTCTGGGTTGG CACACA-3′; forward, 5′-CCAGAGCCAACGTCAAGCAT-3′, and reverse, 5′-CAGCCGTGCAACAATCTGAA-3′. TaqMan primers and 2× Universal TaqMan Fast Master Mix (Applied Biosystems) were used to assess CXCL13, CCL19, CCL21, gamma interferon (IFN-γ), IgG, and CXCR4 mRNAs. Expression levels were compared relative to glyceraldehyde-3-phosphate dehydrogenase (GAPDH) mRNA as described previously (27, 29). Reactions using SYBR green were run under the following conditions: 95°C for 10 min, followed by 40 cycles of denaturation at 94°C for 10 s, annealing at 60°C for 30 s, and elongation at 72°C for 30 s. TaqMan reactions were performed using an ABI 7500 Fast PCR and 7500 software, and reactions were initiated by incubation at 95°C for 20 s, followed by 40 cycles of denaturation at 95°C for 3 s and annealing and extension at 60°C for 30 s. Transcript levels were calculated from triplicate samples relative to the housekeeping gene GAPDH using the following formula: $2[C_T(\text{GAPDH}) - C_T(\text{target gene})] \times 1{,}000$, where C_T is threshold cycle. IFN-γ in cell-free spinal cord supernatants was determined by enzyme-linked immunosorbent assay (ELISA) as described previously (14, 29).

Distribution of CD4$^+$ or CD8$^+$ cells was determined by staining acetone-fixed, 10-μm spinal cord cryosections with Ab specific for CD4 or CD8 (BD Biosciences), followed by incubation with anti-rat IgG (Vector Laboratories, Burlingame, CA). Immunoreactivity was detected by immunoperoxidase staining using a Vectastain ABC kit (Vector Laboratories). ASC distribution was examined using anti-CD138 (Abcam, Cambridge, MA), followed by staining with anti-mouse IgG (38). Immunoreactivity was detected by immunoperoxidase staining using a Vector Mouse on Mouse (M.O.M.) Peroxidase immunodetection kit (Vector Laboratories). Digital images were captured using a Leica DMLB light microscope (Leica Microsystems, Bannockburn, IL) equipped with a SPOT Insight camera (Columbia, IL). Sections were scored, and positive cells were counted in a blinded manner.

RESULTS

Peripheral expansion of CXCR3-expressing ASC precedes CNS accumulation. Following JHMV infection, virus-specific ASC peak in the draining CLN ~1 week prior to accumulating

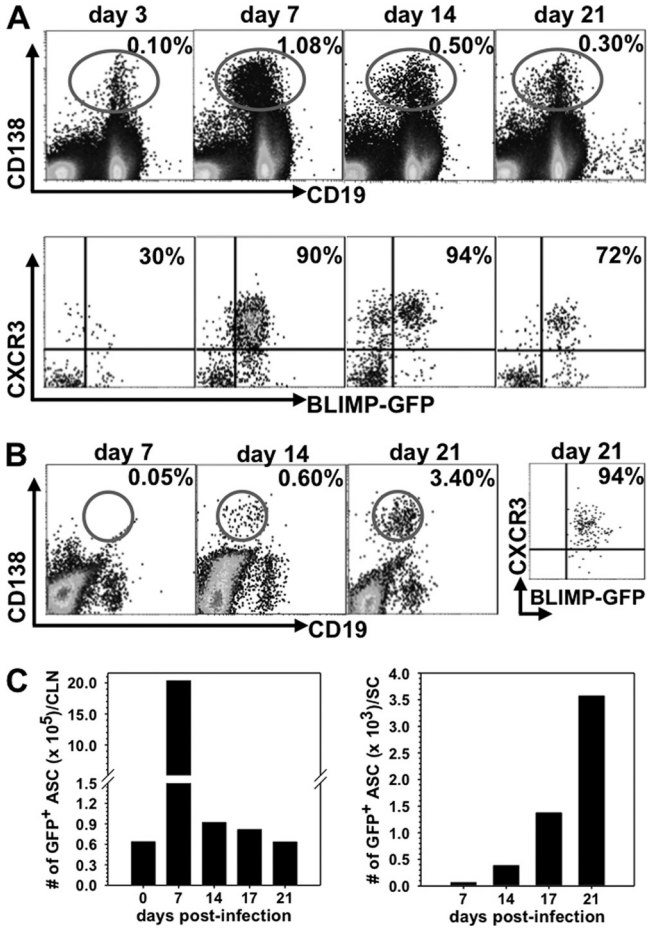

FIG. 1. CXCR3$^+$ ASC expand in CLN prior to CNS infiltration. Cells isolated from CLN and spinal cord of naïve and infected BLIMP-1-GFP$^{+/-}$ mice were analyzed for CD19, CD138, GFP, and CXCR3 expression by flow cytometry. (A) Representative plots of CD138 and CD19 expression on CLN cells (top) and of CXCR3 and GFP expression on CD138$^+$ CLN cells (bottom). Numbers depict the percentage of GFP$^+$ CD138$^+$ cells expressing CXCR3. (B) Spinal cord-infiltrating cells were identified by high levels of CD45 (CD45^{high}) surface expression. Dot plots depict CD138$^+$ CD19$^+$ cells within CD45^{high} infiltrates; the far right plot represents the percentage of CD138$^+$ cells expressing both CXCR3 and GFP at day 21 p.i. (C) Changes of total GFP$^+$ CD138$^+$ ASC in the CLN and spinal cord throughout infection. Data are representative of three experiments with pooled organs from 2 to 4 mice/time point/experiment.

in the CNS at day 21 postinfection (p.i.) (37, 38). Furthermore, expression of the CXCR3 ligands CXCL9 and CXCL10 remains markedly elevated after infectious virus is controlled (27, 38), supporting their potential role as ASC chemoattractants. CXCL11 is excluded due to the nonfunctional gene in C57BL/6 mice (23). Blimp-1-GFP$^{+/-}$ mice (13) were infected to determine CXCR3 expression on peripheral and CNS-recruited ASC, defined by their BLIMP-1$^+$ CD138$^+$ phenotype. Naïve mice contained ~0.1% ASC in both CLN and spleen (data not shown). Infection increased the ASC frequency in CLN to ~1.0% by day 7 p.i., and elevated levels were maintained to day 21 p.i. (Fig. 1A). In contrast, ASC expansion in spleen was minimal, with frequencies of <0.25%, supporting CLN as the primary site of lymphocyte activation (1). Although a small percentage of CD138$^-$ CD19$^+$ B cells in the CLN also expressed BLIMP-1-GFP (Fig. 2), this population was excluded from analysis because GFP expression levels were lower than in the CD138$^+$ population. During peak expansion in the CLN, >90% of CD138$^+$ BLIMP-1$^+$ ASC expressed CXCR3, while <50% expressed CXCR3 in naive mice (data not shown). In the CNS ASC did not accumulate to peak levels until day 21 p.i., with the vast majority (~90%) expressing CXCR3 (Fig. 1B). In contrast to ASC, <8% of CD138$^-$ CD19$^+$ B cells expressed CXCR3 at any time p.i. in either the periphery (Fig. 2) or CNS (data not shown), suggesting that CXCR3 upregulation was mainly restricted to ASC. Kinetic analysis of ASC per organ revealed an ~30-fold increase within the first 7 days p.i. in CLN, which subsequently declined as ASC began emerging in the CNS at day 14 p.i. (Fig. 1C). CXCR4 expression, associated with bone marrow homing, paralleled CXCR3 expression on ASC in both the CLN (Fig. 2) and CNS (data not shown). Similar to CXCR3, CXCR4 expression also remained relatively constant at 7 to 10% on CD138$^-$ CD19$^+$ B cells in the CLN (Fig. 2). The early expansion of CXCR3$^+$ ASC in CLN prior to detection of virus-specific ASC in lymphoid organs (37) indicated nonspecific, cytokine-mediated proliferation; nevertheless, their delayed CNS accumulation mirrored the kinetics of virus-specific ASC (37). These data supported either CXCR3- or CXCR4-mediated ASC release from the CLN and migration to the CNS during viral encephalomyelitis.

CXCR3 deficiency diminishes survival during persistence without impairing peripheral humoral immunity. Demonstration of a direct link between CXCR3 and ASC migration to inflamed nonlymphoid tissues is complicated by potential migratory effects on other lymphocytes, as CXCR3 regulates NK and T cell recruitment, depending on the experimental model (23). However, there is no evidence for a role of NK cells during JHMV infection (41). Furthermore, anti-CXCR3 Ab treatment of mice infected with a lethal JHMV variant primarily affected CD4$^+$ T cell migration to the CNS but did not alter mortality onset or survival rate (35). As CD8$^+$ T cells are the primary antiviral effectors during acute infection with sublethal JHMV (1, 29), we anticipated survival of CXCR3$^{-/-}$ mice to be minimally compromised prior to the time of ASC accumulation. Indeed, clinical disease progression was comparable between CXCR3$^{-/-}$ and wild-type (WT) mice during the first 14 days p.i. (Fig. 3). However, disease severity increased strikingly in CXCR3$^{-/-}$ mice after day 18 p.i., similar to enhanced disease progression in B cell-deficient mice (17, 32). Low mortality in infected CXCR3$^{-/-}$ mice at the time of peak virus-specific CNS ASC accumulation in WT controls (38) thus permitted comparative analysis of ASC migration.

To ensure that CXCR3 deficiency does not alter peripheral ASC activation following CNS infection, virus-specific as well as total ASC were first examined in CLN. CXCR3$^{-/-}$ mice exhibited 2- to 3-fold increased frequencies of total IgG-secreting ASC at day 21 p.i., but differences from the WT level resolved by day 28 p.i. (Fig. 4A). Similarly, the frequency of virus-specific ASC was prominently elevated at day 21 and to a lesser extent at day 28 p.i. (Fig. 4A). Following peripheral infections or vaccination, CXCR4 signaling attracts a fraction of antigen-specific ASC into bone marrow, where they survive as long-lived ASC maintaining serum Ab (21, 35, 36). Assess-

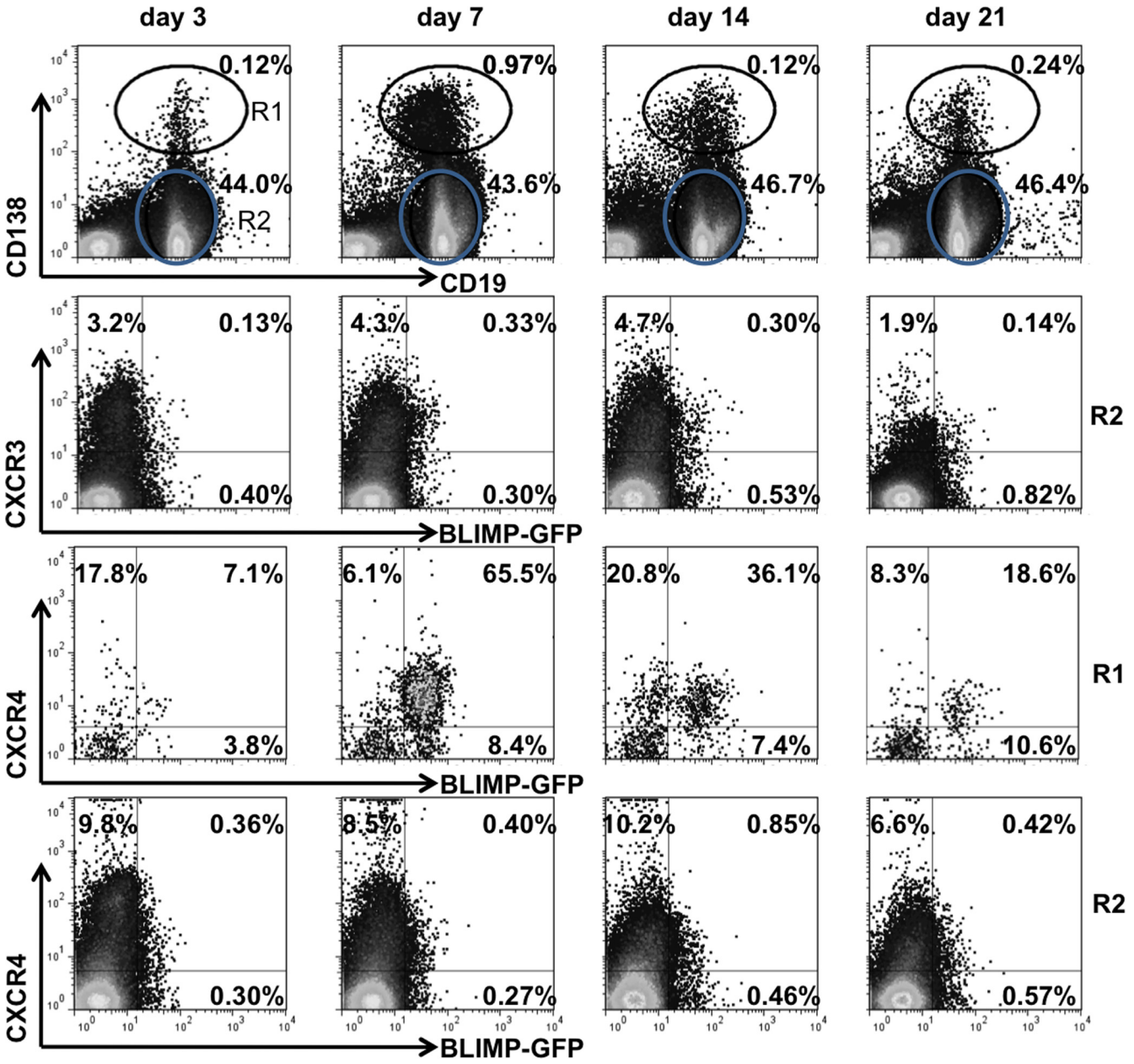

FIG. 2. CXCR3 and CXCR4 expression on B cells in CLN following virus infection. Cells isolated from CLN of infected BLIMP-1-GFP$^{+/-}$ mice were analyzed for CD19, CD138, GFP, CXCR3, and CXCR4 expression by flow cytometry at the indicated times p.i. Representative plots depict CD138^{+} CD19^{lo} cells in the R1 region and CD138^{-} CD19^{+} B cells in the R2 gate with relative percentages (first row), CXCR3 and GFP expression on CD138^{-} CD19^{+} cells (R2) (second row), and CXCR4 and GFP expression on CD138^{+} CD19^{lo} cells (R1) and CD138^{-} CD19^{+} cells (R2) (third and fourth rows, respectively). Numbers in quadrants depict relative percentages in each quadrant. Data are representative of three experiments with pooled CLN from 2 to 4 mice/time point/experiment.

ment of virus-specific ASC in bone marrow, to ensure that migration to bone marrow was not affected during CNS infection, revealed even higher ASC frequencies in CXCR3$^{-/-}$ mice than in WT mice between days 14 and 21 p.i. (Fig. 4B). Uncompromised migration to bone marrow thus eliminated a role for CXCR3 in ASC egress from the CLN. These results predicted that peripheral humoral responses were not impaired. Indeed, no differences in either virus-specific or neutralizing Ab were detected in infected CXCR3$^{-/-}$ mice and WT mice (Fig. 4C). CXCR3 was thus dispensable for virus-specific ASC expansion, differentiation, and trafficking to bone marrow following JHMV infection.

CXCR3 is required for ASC migration into the virus-infected CNS. Following JHMV infection, virus-specific ASC populations are comprised of IgA, IgM, and IgG secretors, which all emerge in the CNS at days 14 to 15 p.i. (35). Due to the dominance of IgG ASC by day 21 p.i. and the protective nature of IgG neutralizing Ab in this model (31, 37), analysis

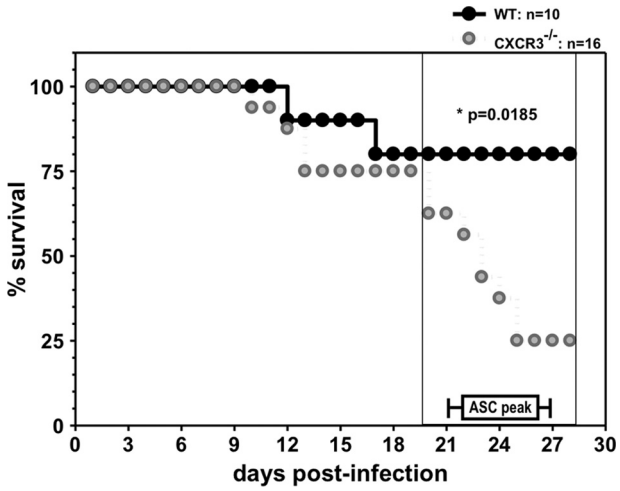

FIG. 3. CXCR3 deficiency increases mortality during persistent infection. CXCR3$^{-/-}$ and WT mice were infected with JHMV and monitored daily for disease progression. The percentage of surviving mice is shown for one experiment representative of three experiments with a minimum of 10 mice/group. Peak virus-specific ASC accumulation in WT mice (37, 38) is indicated for reference.

focused on the IgG response. Evaluation of CXCR3 as a mediator of ASC recruitment into the CNS revealed a >90% reduction in virus-specific ASC in CXCR3$^{-/-}$ mice (Fig. 5A). Both ELISPOT as well as flow cytometric analysis of CD138^{+} ASC frequencies (Fig. 5A and B) further revealed that impaired recruitment not only was specific for virus-specific ASC but also affected total IgG secreting cells. To directly assess the effect of impaired ASC accumulation on virus-specific Ab within the CNS, spinal cord supernatants were assessed for both virus-specific IgM and IgG levels. Figure 5C demonstrates prominent accumulation of both IgM and IgG in the CNS of WT mice by day 21 p.i., with IgG levels vastly exceeding IgM. In contrast, although both virus-specific IgM and IgG were detectable in CXCR3$^{-/-}$ mice, levels were significantly reduced compared to those in WT mice. Measurement of total IgG mRNA levels in the CNS further confirmed a severe deficit in total IgG production. These data demonstrated an essential role for CXCR3 ligands in mediating ASC migration to the CNS during viral encephalomyelitis, independent of Ig isotype secretion.

In addition to expressing CXCR4, a subset of plasma blasts is also characterized by CXCR2 mRNA expression after lipopolysaccharide (LPS) stimulation (13). While CXCR4 functions in leukocyte migration to, as well as retention in, bone

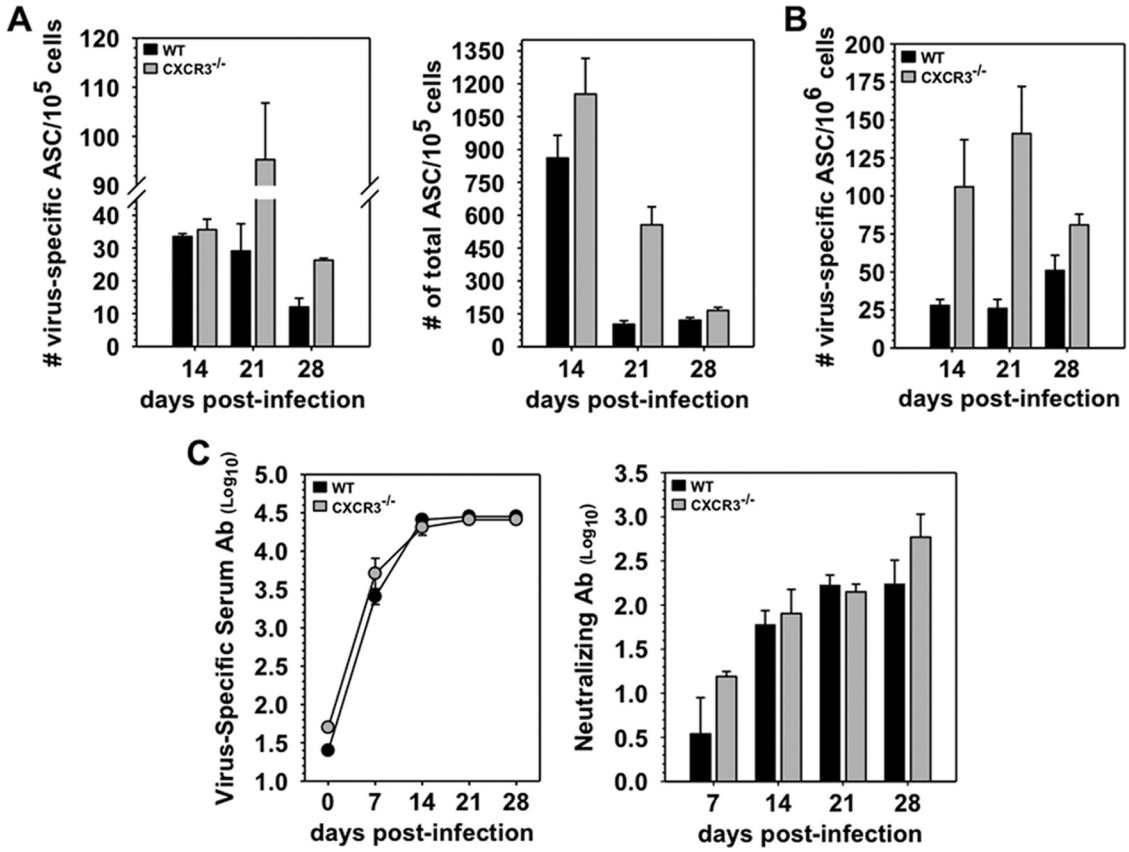

FIG. 4. Normal peripheral humoral responses in CXCR3$^{-/-}$ mice. (A) Frequencies of virus-specific and total IgG-secreting ASC in CLN measured by ELISPOT assay. (B) ELISPOT analysis of virus-specific ASC in bone marrow, representative of three experiments with pooled samples from 4 to 6 mice/time point. (C) Virus-specific IgG2a and virus neutralizing Ab in sera of infected WT and CXCR3$^{-/-}$ mice. IgG2a titers are the average of triplicate samples from three individual mice per time point. Neutralizing titers from pooled serum (n = 3 to 5 mice/time point/experiment) reflect the average titers from two to three experiments.

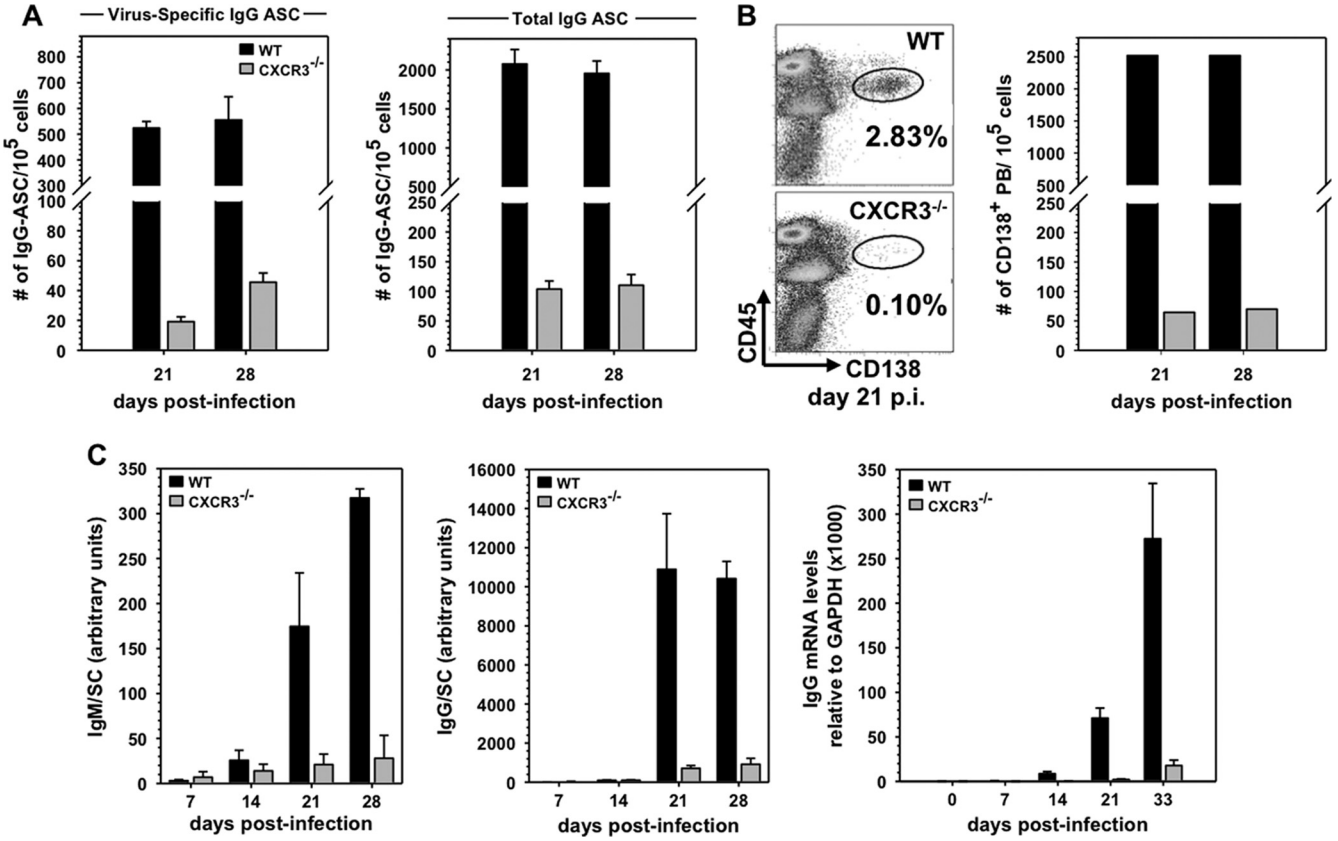

FIG. 5. CXCR3 is required for ASC accumulation in the CNS. (A) ELISPOT assay-derived frequencies of virus-specific and total IgG-ASC in spinal cords of WT and CXCR3$^{-/-}$ mice at days 21 and 28 p.i. (B) Representative flow cytometry density plots of CD138^{+} ASC derived from spinal cords of WT and CXCR3$^{-/-}$ mice at day 21 p.i. (left) and a representative bar graph depicting reduced frequencies of CD138^{+} ASC in spinal cords of CXCR3$^{-/-}$ mice (right). Data are representative of three experiments with 4 to 6 mice/time point. (C) Virus-specific IgM and IgG2a in supernatants from spinal cord homogenates of infected WT and CXCR3$^{-/-}$ mice assessed by ELISA (left and middle panels). Arbitrary units reflect total Ab levels per spinal cord from three individual mice per time point. Background values from naïve mice were subtracted. IgG mRNA values represent average expression levels relative to GAPDH ± standard error of the mean from three individual mice/time point (right panel).

marrow, CXCR2 has mainly been implicated in neutrophil migration out of the bone marrow (4). To rule out a potential contribution of altered CXCR4 or CXCR2 expression to impaired ASC CNS migration in the absence of CXCR3, expression of these chemokine receptors was assessed in CLN-derived ASC during their peak expansion. CXCR4 expression levels were similar on CD138^{+} ASC in WT (50.8% ± 3.8%) and CXCR3$^{-/-}$ (54% ± 4.5%) mice at day 7 p.i. (data not shown). At day 10 p.i. the percentages increased to ~62% in WT mice and decreased to ~38% in CXCR3$^{-/-}$ mice (Fig. 6A). In contrast, we found no evidence for CXCR2 expression on WT or CXCR3$^{-/-}$ ASC at days 7 or 10 p.i. (Fig. 6A; also data not shown). However, CXCR2 was readily detectable on splenic neutrophils in both groups of infected mice (Fig. 6B), confirming that there was no overall defect in CXCR2 regulation. Impaired migration of CXCR3$^{-/-}$ ASC to the CNS thus did not coincide with significantly dysregulated CXCR2 or CXCR4 expression.

To further rule out potential indirect effects of diminished CNS CD4^{+} T cells on ASC accumulation, as suggested by CXCL10 blockade (19), T cell CNS infiltration was also monitored. However, no differences in CD4^{+}, CD8^{+}, or virus-specific CD8^{+} T cell levels were detected in CXCR3$^{-/-}$ and WT mice during acute infection (Fig. 7A). Equivalent IFN-γ levels in the CNS further supported similar viral antigen-driven T cell responses throughout infection (Fig. 7B). Interleukin-21 (IL-21), a cytokine known to enhance CD8^{+} T cell effector function as well as humoral responses, was recently shown to be predominantly produced by CD4 T cells during JHMV encephalomyelitis (27). Although IL-21 mRNA was reduced in the CNS of CXCR3$^{-/-}$ mice at day 7 p.i., levels were similar by day 14 p.i. and thereafter (Fig. 7C). These data supported the idea that T cell migration to and function within the CNS were not significantly impaired in the absence of CXCR3. To confirm effective antiviral T cell function during the acute phase of infection and assess the biological consequences of diminished virus-specific ASC within the CNS, viral control was examined by monitoring mRNA encoding the viral nucleocapsid protein (27, 29). Similar reductions in viral RNA between days 7 and 14 p.i. in both groups supported effective T cell-mediated clearance in the absence of CXCR3 (Fig. 7D). Nevertheless, the CNS of infected CXCR3$^{-/-}$ mice harbored elevated viral RNA at day 21 p.i. coinciding with increased mortality. Elevated viral RNA in CXCR3$^{-/-}$ mice was consistent with the sustained presence of infectious virus at both day 21 and day 28 p.i. in surviving mice, which remained undetectable or near

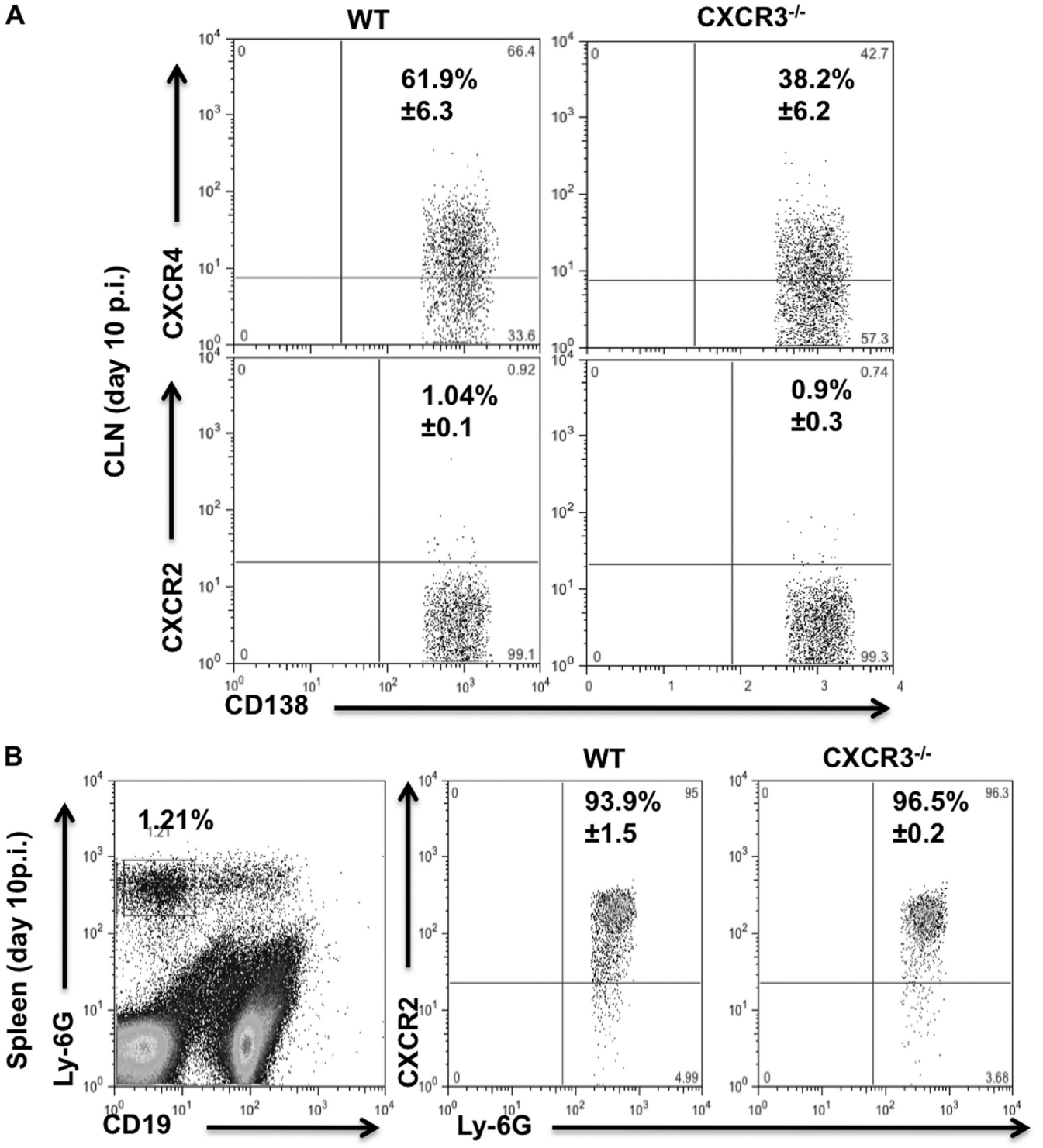

FIG. 6. ASC do not express CXCR2 but maintain CXCR4 expression even in the absence of CXCR3. Cells isolated from CLN and spleen of JHMV-infected WT and CXCR3$^{-/-}$ mice were analyzed for CD19, CD138, Ly-6G, CXCR4, and CXCR2 expression by flow cytometry at day 10 p.i. (A) Representative plots demonstrating CXCR4, but not CXCR2, expression on ASC. Gates were set on CD138^{+} CD19^{lo} ASC as depicted by the R1 region in Fig. 2. Numbers depict mean percentages ± standard deviations of ASC expressing CXCR4 or CXCR2, as indicated. (B) CXCR2 staining was validated on splenic neutrophils identified by reactivity with anti Ly-6G MAb. The left plot depicts the percentage of Ly-6G^{+} CD19^{-} neutrophils in total WT splenocytes at day 10 p.i. The middle and right plots demonstrate CXCR2 expression on cells in the neutrophil gate. Numbers depict mean percentages ± standard deviations of neutrophils expressing CXCR2. In both panels, quadrants were set based on staining with an isotype control MAb. Data are derived from three individual mice per time point.

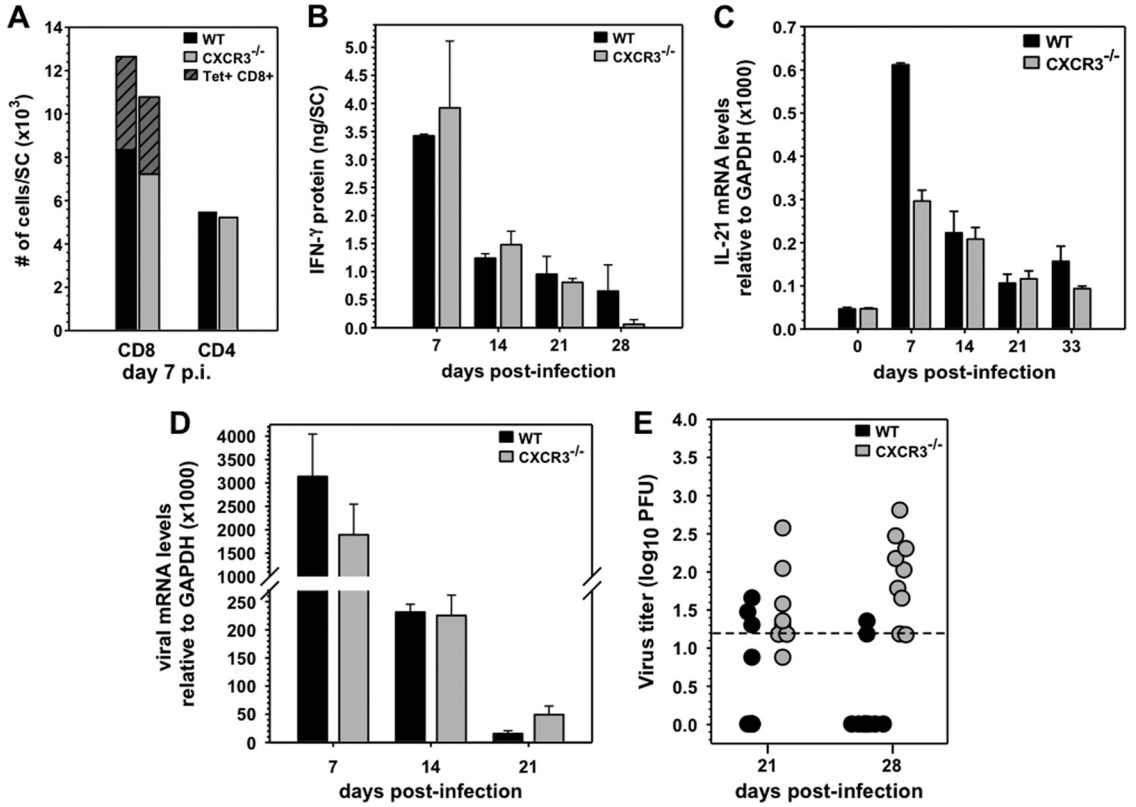

FIG. 7. CXCR3 deficiency impairs virus control during persistence independent of T cells. (A) Accumulation of total $CD8^+$, Db-S510 tetramer-positive $CD8^+$ (striped portion), and $CD4^+$ T cells per spinal cord as assessed by flow cytometry at day 7 p.i. Data are from 4 mice/group and are representative of three experiments. (B) Average IFN-γ protein ± standard errors of the means in spinal cords of virus-infected mice (n = 3 per time point). (C) Average expression levels of IL-21 mRNA in spinal cords relative to GAPDH ± standard errors of the means from three individual mice/time point. Panels D and E show viral mRNA and infectious virus levels, respectively, in spinal cords of infected mice. The dashed line indicates the limit of detection.

the detection level in the majority of WT mice after 14 days p.i. (Fig. 7E).

These results demonstrated no obvious defects in CNS T cell recruitment and function, in contrast with Ab-mediated CXCR3 ligand blocking studies (19). The anatomical distributions of T cells and ASC were thus analyzed in spinal cords persistently infected with JHMV to assess their parenchymal localization (Fig. 8). Significantly fewer $CD138^+$ ASC were present in spinal cords of $CXCR3^{-/-}$ mice than in WT mice (5 ± 6.4 in $CXCR3^{-/-}$ versus 140 ± 93 cells/mm^2 in WT). This reduction amounted to >95%, consistent with both flow cytometric and functional ELISPOT analysis and ELISA. The exceptionally rare ASC in $CXCR3^{-/-}$ spinal cords were all perivascular, with none detected in the parenchyma. T cells in WT mice preferentially accumulated in white matter tracts, while their distribution was more diffuse in $CXCR3^{-/-}$ mice. However, both $CD4^+$ (172 ± 16 cells/mm^2 in WT versus 165 ± 103 cells/mm^2 in $CXCR3^{-/-}$) and $CD8^+$ (340 ± 17 cells/mm^2 in WT versus 323 ± 39 cells/mm^2 in $CXCR3^{-/-}$) T cell levels were comparable (Fig. 8). As serum neutralizing Abs were similar in both groups, these data demonstrate the critical role of intrathecal ASC in contributing to viral control during persistence.

To further support the direct requirement of CXCR3 for ASC migration to the inflamed CNS, dysregulation of alternative signals potentially contributing to defective ASC accumulation was excluded by comparing CXCL12, CXCL13, CCL19, and CCL21 mRNA levels (Fig. 9); all four chemokines are associated with *de novo* lymphoid neogenesis, which plays a role in supporting ongoing humoral responses during chronic autoimmune-driven inflammation (13, 18, 20). CXCL9 and CXCL10 were included to validate similar IFN-γ-dependent expression given the IFN-γ defect in $CXCR3^{-/-}$ mice with experimental autoimmune encephalomyelitis (18). CXCL9, CXCL10, and CXCL12 mRNA levels were comparable, if not increased in the CNS of $CXCR3^{-/-}$ mice, suggesting that chemokines associated with ASC migration are not impaired or dysregulated. CXCR4 mRNA levels were also similar in the CNS of both groups (data not shown), indicating no gross dysregulation of the CXCL12 receptor. A contribution of CXCR2 to ASC migration, implicated by *in vitro* stimulation of ASC (13), was already questioned by the absence of CXCR2 expression on ASC following CNS infection (Fig. 6). Similarly high levels of mRNA encoding CXCR2 ligands CXCL1 and CXCL2 in the CNS at day 7 p.i. in both groups, followed by a rapid decline by day 14 p.i. (data not shown), further negated a role for CXCR2 in ASC recruitment to the CNS. CXCL13, expressed constitutively in lymphoid tissue (15), was undetectable in the naive CNS but was present at day 7 p.i. and remained elevated to day 21 p.i., confirming recent results (27).

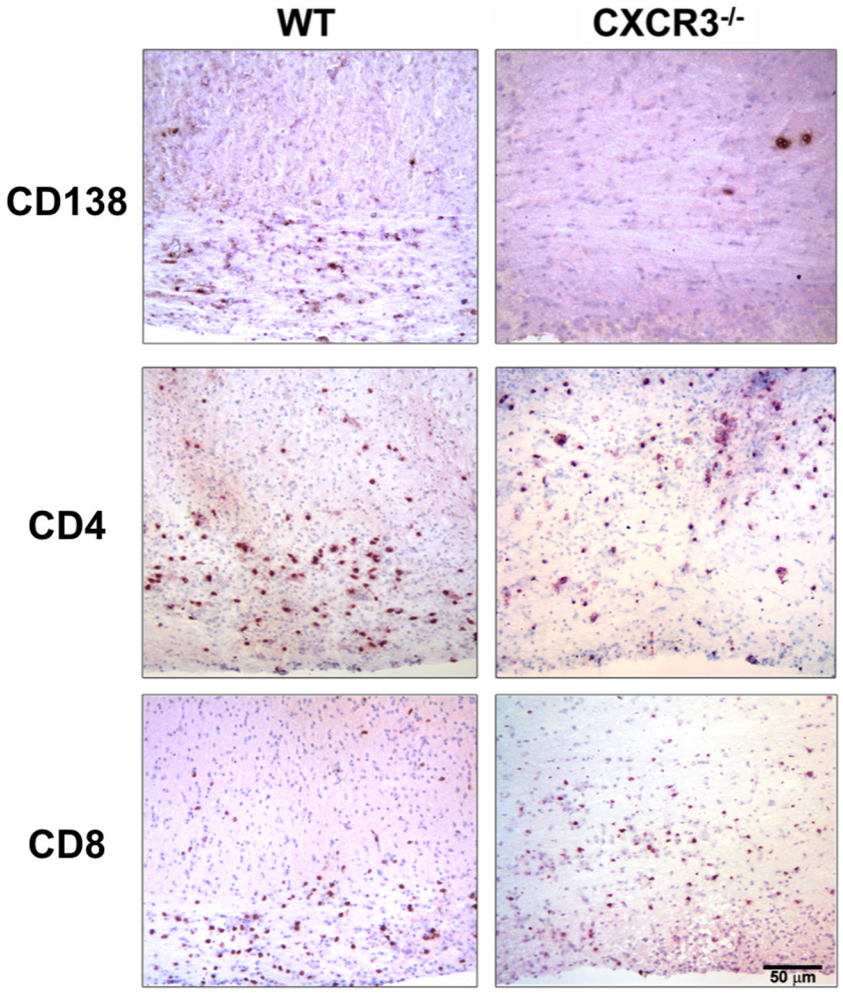

FIG. 8. CXCR3 deficiency specifically reduces CNS accumulation of $CD138^+$ cells. Immunohistochemical analysis of $CD138^+$, $CD4^+$, and $CD8^+$ lymphocytes in virus-infected spinal cords at day 22 p.i. (3 mice/group). Bar, 50 μm.

Elevated CXCL13 in the CNS during inflammation is likely due to expression by recruited dendritic cells. Whether the CXCL13 decline in $CXCR3^{-/-}$ mice has functional significance remains unclear. Lastly, CCL19 and CCL21 mRNAs were both detectable in the CNS of naïve WT and $CXCR3^{-/-}$ mice. Although CCL19 mRNA increased during acute infection, the level varied by only ~2-fold at day 7 p.i. in $CXCR3^{-/-}$ mice. Surprisingly, the basal CCL21 mRNA level in the CNS was ~40-fold higher in $CXCR3^{-/-}$ mice than in WT mice. Nevertheless, infection did not alter the respective basal levels in either group. Similar or higher expression of CXCL13, CCL19, and CCL21 mRNAs in the CNS of $CXCR3^{-/-}$ mice, corresponding to the time of ASC recruitment in WT mice, suggests that these chemokines do not make a major contribution to ASC CNS accumulation during JHMV encephalomyelitis.

DISCUSSION

CNS-localized ASC or Abs in cerebral spinal fluid are a hallmark of numerous microbial CNS infections in both murine models and humans (8, 11, 24, 25, 40). While Abs can diffuse across a compromised blood brain barrier, prolonged detection of ASC and oligoclonal Ab bands favor local Ab secretion by ASC. Although their role in human infections cannot be assessed easily, murine models of rabies virus, neurotropic coronavirus, and alpha viruses all suggest an effective, nonlytic strategy of CNS viral control (6, 11, 16, 31). However, the signals mediating CNS ASC accumulation and the contribution of ASC to protection are poorly characterized. Herein, we demonstrate an essential role for CXCR3 in regulating ASC migration to the CNS following virus-induced encephalomyelitis. More importantly, local ASC maintenance is vital to control persistent virus, even in the presence of intact peripheral humoral immunity.

The implication of CXCR3-mediated ASC recruitment from peripheral lymphoid tissue to sustain local humoral immunity is distinct from ectopic lymphoid follicle formation observed during chronic autoimmune inflammation (7, 25). Although a contribution of ectopic lymphoid-like structures to CNS humoral immunity cannot be excluded, neither IgG^+ nor $CD138^+$ cell distribution provided evidence for focal clustering at day 21 p.i. or later during viral persistence (38). This is supported by redundancy in CXCL13 for CNS B cell recruit-

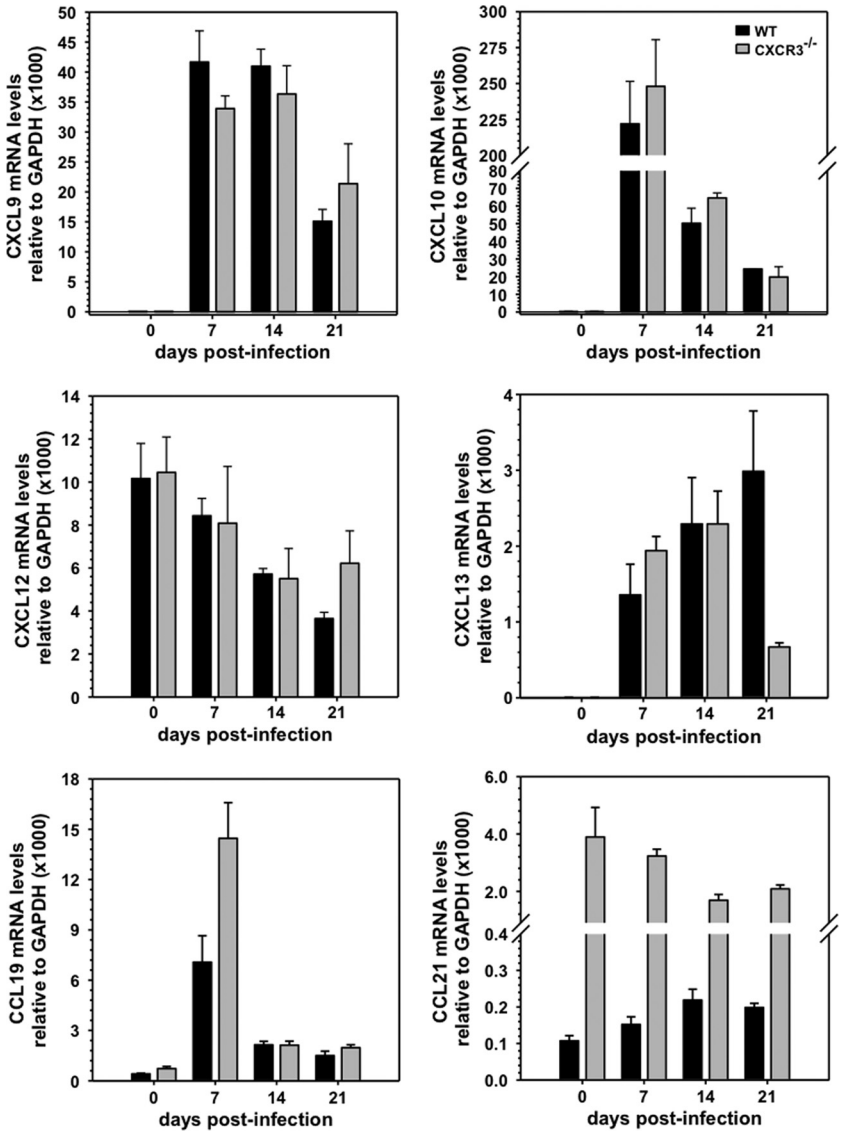

FIG. 9. Expression kinetics and relative levels of chemokines in spinal cords of infected CXCR3$^{-/-}$ and WT mice. Values represent average chemokine mRNA expression levels relative to GAPDH ± standard errors of the means from three individual mice/time point at indicated days p.i.

ment during Sindbis virus encephalitis and experimental allergic encephalomyelitis (30). Moreover, the ASC survival factors BAFF and APRIL are expressed by astrocytes during JHMV infection, providing parenchymal support to maintain ASC within the CNS (27).

The apparent redundancy of CXCR3 for T cell recruitment was similar to unaltered leukocyte migration during CD4$^+$ T cell-mediated experimental autoimmune encephalomyelitis in CXCR3$^{-/-}$ mice (19). In that model, however, T cell deficiencies were implied by reduced IFN-γ expression, which was not evident in our studies. Discrepancies with previous studies relating to T cell CNS recruitment (19, 35) may reside in the distinct methodologies used to disrupt CXCR3-ligand interactions, e.g., Ab blockade, differences in virus variants or dose, or T cell activation state. The results of this study add to incongruent reports demonstrating that the requirement of CXCR3 for T cell trafficking varies depending upon the model (23). The strong implication that CXCR3 directly mediates ASC recruitment to the CNS was further supported by the observation that expression levels of CXCR4 on CXCR3$^{-/-}$ and WT ASC were similar overall during the time of peak expansion. Moreover, CXCR2 expression, which may be a marker of a subset of LPS-stimulated plasma blasts at the transcriptional level, was not detected on CLN-derived ASC in either group. While these data negated a role of CXCR2 in ASC migration, a contribution of CXCR4 cannot be excluded based on its complex role in egress, migration, and retention. The fate of leukocyte circulation and tissue retention can be governed by multiple factors, the regulation of which can be extremely complex (2, 4, 36). Irrespective of the likelihood that additional forces are driving lymphocyte homing, CXCR3-dependent ASC migration *in vivo*, in the absence of overt T cell altera-

tions, enforces the biological relevance of CXCR3-mediated ASC migration *in vitro* (10). Elevated levels of CXCR3 ligands not only may be associated with JHMV persistence but also may characterize numerous other infectious and chronic inflammatory conditions with ongoing IFN-γ expression (39).

Similar to antigen-independent recruitment of T cells to sites of infection, our data further imply that elevated levels of CXCR3 ligands at inflamed sites provide migratory signals for ASC, independent of specificity. However, delayed ASC accumulation in the CNS relative to peak CXCR3 ligand expression, coupled with peripheral $CD138^+$ $CXCR3^+$ ASC expansion, suggests a requirement for additional cues, potentially imprinted during germinal center differentiation. This notion is supported by the narrow window of ASC responsiveness to CXCR4 and CXCR3 ligands *in vitro* (10). A crucial factor contributing to emigration of ASC from lymphoid tissue *in vivo* is the sphingosine 1-phosphate 1 receptor (S1P1), a G protein-coupled receptor required for lymphocyte egress into the circulating bloodstream (12). During secondary immunization, antigen-specific ASC in the blood were distinguished from their splenic counterparts by higher S1P1 and lower CXCR4 expression levels. These results implicated differential S1P1 signaling in determining ASC egress and migration to bone marrow rather than retention in secondary lymphoid tissue (12). The relative signaling through S1P1 and chemokine receptors is thus likely to similarly regulate ASC egress and subsequent migration during primary responses elicited by viral infection. Our results also imply that CXCR3 and CXCR4 receptors differentially regulate ASC homing depending on ligand expression at respective distal sites. Overall, these data demonstrate ASC recruitment as a direct pathway sustaining humoral responses within the CNS and highlight the relevance of ASC in suppressing persisting virus under conditions when T cell immunity is ineffective.

ACKNOWLEDGMENTS

This work was supported by National Institutes of Health grant AI 47249 and National Multiple Sclerosis Society grant RG 3808.

We thank Wenqiang Wei, Ernesto Baron, and Mi Widness for excellent technical assistance.

REFERENCES

1. **Bergmann, C. C., T. E. Lane, and S. A. Stohlman.** 2006. Coronavirus infection of the central nervous system: host-virus stand-off. Nat. Rev. Microbiol. **4:**121–132.
2. **Cruz-Orengo, L., et al.** 2011. CXCR7 influences leukocyte entry into the CNS parenchyma by controlling abluminal CXCL12 abundance during autoimmunity. J. Exp. Med. **208:**327–339.
3. **Cyster, J. G.** 2003. Homing of antibody secreting cells. Immunol. Rev. **194:** 48–60.
4. **Eash, K. J., A. M. Greenbaum, P. K. Gopalan, and D. C. Link.** 2010. CXCR2 and CXCR4 antagonistically regulate neutrophil trafficking from murine bone marrow. J. Clin. Invest. **120:**2423–2431.
5. **Fleming, J. O., M. D. Trousdale, F. A. el-Zaatari, S. A. Stohlman, and L. P. Weiner.** 1986. Pathogenicity of antigenic variants of murine coronavirus JHM selected with monoclonal antibodies. J. Virol. **58:**869–875.
6. **Fragkoudis, R., C. M. Ballany, A. J. K. Boyd, and Fazakerley.** 2008. In Semliki Forest virus encephalitis, antibody rapidly clears infectious virus and is required to eliminate viral material from the brain, but is not required to generate lesions of demyelination. J. Gen. Virol. **89:**2565–2568.
7. **Franciotta, D., M. Salvetti, F. Lolli, B. Serafini, and F. Aloisi.** 2008. B cells and multiple sclerosis. Lancet Neurol. **7:**852–858.
8. **Griffin, D., B. Levine, W. Tyor, S. Ubol, and P. Despres.** 1997. The role of antibody in recovery from alphavirus encephalitis. Immunol. Rev. **159:**155–161.
9. **Hargreaves, D. C., et al.** 2001. A coordinated change in chemokine responsiveness guides plasma cell movements. J. Exp. Med. **194:**45–56.
10. **Hauser, A. E., et al.** 2002. Chemotactic responsiveness toward ligands for CXCR3 and CXCR4 is regulated on plasma blasts during the time course of a memory immune response. J. Immunol. **169:**1277–1282.
11. **Hooper, D. C., T. W. Phares, M. J. Fabis, and A. Roy.** 2009. The production of antibody by invading B cells is required for the clearance of rabies virus from the central nervous system. PLoS Negl. Trop. Dis. **3:**e535.
12. **Kabashima, K., et al.** 2006. Plasma cell S1P1 expression determines secondary lymphoid organ retention versus bone marrow tropism. J. Exp. Med. **203:**2683–2690.
13. **Kallies, A., et al.** 2004. Plasma cell ontogeny defined by quantitative changes in blimp-1 expression. J. Exp. Med. **200:**967–977.
14. **Kapil, P., et al.** 2009. Interleukin-12 (IL-12), but not IL-23, deficiency ameliorates viral encephalitis without affecting viral control. J. Virol. **83:**5978–5986.
15. **Lalor, S. J., and B. M. Segal.** 2010. Lymphoid chemokines in the CNS. J. Neuroimmunol. **224:**56–61.
16. **Levine, B., et al.** 1991. Antibody-mediated clearance of alphavirus infection from neurons. Science **254:**856–860.
17. **Lin, M. T., D. R. Hinton, N. W. Marten, C. C. Bergmann, and S. A. Stohlman.** 1999. Antibody prevents virus reactivation within the central nervous system. J. Immunol. **162:**7358–7368.
18. **Liu, L., et al.** 2006. Severe disease, unaltered leukocyte migration, and reduced IFN-gamma production in $CXCR3^{-/-}$ mice with experimental autoimmune encephalomyelitis. J. Immunol. **176:**4399–4409.
19. **Liu, M. T., H. S. Keirstead, and T. E. Lane.** 2001. Neutralization of the chemokine CXCL10 reduces inflammatory cell invasion and demyelination and improves neurological function in a viral model of multiple sclerosis. J. Immunol. **167:**4091–4097.
20. **Luther, S. A., et al.** 2002. Differing activities of homeostatic chemokines CCL19, CCL21, and CXCL12 in lymphocyte and dendritic cell recruitment and lymphoid neogenesis. J. Immunol. **169:**424–433.
21. **Manz, R. A., A. E. Hauser, F. Hiepe, and A. Radbruch.** 2005. Maintenance of serum antibody levels. Annu. Rev. Immunol. **23:**367–386.
22. **Muehlinghaus, G., et al.** 2005. Regulation of CXCR3 and CXCR4 expression during terminal differentiation of memory B cells into plasma cells. Blood **105:**3965–3971.
23. **Muller, M., S. Carter, M. J. Hofer, and I. L. Campbell.** 2010. Review: the chemokine receptor CXCR3 and its ligands CXCL9, CXCL10 and CXCL11 in neuroimmunity—a tale of conflict and conundrum. Neuropathol. Appl. Neurobiol. **36:**368–387.
24. **Norrby, E.** 1977. Characterization of the virus antibody activity of oligoclonal IgG produced in the central nervous system of patients with multiple sclerosis, p. 150–164. *In* V. ter Meulen and M. Katz (ed.), Slow virus infections in the central nervous system. Springer Verlag, New York, NY.
25. **Owens, G. P., J. L. Bennett, D. H. Gilden, and M. P. Burgoon.** 2006. The B cell response in multiple sclerosis. Neurol. Res. **28:**236–244.
26. **Pachner, A. R., J. Brady, and K. Narayan.** 2007. Antibody-secreting cells in the central nervous system in an animal model of MS: phenotype, association with disability, and in vitro production of antibody. J. Neuroimmunol. **190:** 112–120.
27. **Phares, T. W., C. P. Marques, S. A. Stohlman, D. R. Hinton, and C. C. Bergmann.** 2011. Factors supporting intrathecal humoral responses following viral encephalomyelitis. J. Virol. **85:**2589–2598.
28. **Phares, T. W., et al.** 2009. Target-dependent B7–H1 regulation contributes to clearance of central nervous system infection and dampens morbidity. J. Immunol. **182:**5430–5438.
29. **Phares, T. W., S. A. Stohlman, D. R. Hinton, R. Atkinson, and C. C. Bergmann.** 2010. Enhanced antiviral T cell function in the absence of B7—H1 is insufficient to prevent persistence but exacerbates axonal bystander damage during viral encephalomyelitis. J. Immunol. **185:**5607–5618.
30. **Rainey-Barger, E. K., et al.** 2010. The lymphoid chemokine, CXCL13, is dispensable for the initial recruitment of B cells to the acutely inflamed central nervous system. Brain Behav. Immun. [Epub ahead of print.] doi: 10.1016/j.bbi.2010.10.002.
31. **Ramakrishna, C., C. C. Bergmann, R. Atkinson, and S. A. Stohlman.** 2003. Control of central nervous system viral persistence by neutralizing antibody. J. Virol. **77:**4670–4678.
32. **Ramakrishna, C., S. A. Stohlman, R. D. Atkinson, M. J. Shlomchik, and C. C. Bergmann.** 2002. Mechanisms of central nervous system viral persistence: the critical role of antibody and B cells. J. Immunol. **168:**1204–1211.
33. **Shapiro-Shelef, M., and K. Calame.** 2005. Regulation of plasma-cell development. Nat. Rev. Immunol. **5:**230–242.
34. **Slifka, M. K., R. Antia, J. K. Whitmire, and R. Ahmed.** 1998. Humoral immunity due to long-lived plasma cells. Immunity **8:**363–372.
35. **Stiles, L. N., M. P. Hosking, R. A. Edwards, R. M. Strieter, and T. E. Lane.** 2006. Differential roles for CXCR3 in $CD4^+$ and $CD8^+$ T cell trafficking following viral infection of the CNS. Eur. J. Immunol. **36:**613–622.
36. **Tokoyoda, K., A. E. Hause, T. T. Nakrayama, A. Radbruch.** 2010. Organization of immunological memory by bone marrow stroma. Nat. Rev. Immunol. **10:**193–200.
37. **Tschen, S. I., et al.** 2002. Recruitment kinetics and composition of antibody-

secreting cells within the central nervous system following viral encephalomyelitis. J. Immunol. **168:**2922–2929.
38. **Tschen, S. I., et al.** 2006. CNS viral infection diverts homing of antibody-secreting cells from lymphoid organs to the CNS. Eur. J. Immunol. **36:**603–612.
39. **Tsubaki, T., et al.** 2005. Accumulation of plasma cells expressing CXCR3 in the synovial sublining regions of early rheumatoid arthritis in association with production of Mig/CXCL9 by synovial fibroblasts. Clin. Exp. Immunol. **141:**363–371.
40. **Tyor, W. R., and D. E. Griffin.** 1993. Virus specificity and isotype expression of intraparenchymal antibody-secreting cells during Sindbis virus encephalitis in mice. J. Neuroimmunol. **48:**37–44.
41. **Zuo, J., et al.** 2006. Mouse hepatitis virus pathogenesis in the central nervous system is independent of IL-15 and natural killer cells. Virology **350:**206–215.